Strongly Interacting Rydberg Excitations of a Cold Atomic Gas

Y. O. Dudin and A. Kuzmich*

Highly excited Rydberg atoms have many exaggerated properties. In particular, the interaction strength between such atoms can be varied over an enormous range. In a mesoscopic ensemble, such strong, long-range interactions can be used for fast preparation of desired many-particle states. We generated Rydberg excitations in an ultra-cold atomic gas and subsequently converted them into light. As the principal quantum number n was increased beyond ~70, no more than a single excitation was retrieved from the entire mesoscopic ensemble of atoms. These results hold promise for studies of dynamics and disorder in many-body systems with tunable interactions and for scalable quantum information networks.

A quantum many-particle system in which interactions can be tuned over a vast range may enable profound changes in the way we understand and explore physics of the microscopic realm (*1*). For example, it may lead to previously unknown phases of matter and aid in the discovery of new phenomena. Strong coupling allows for fast, controllable many-body dynamics, whereas the weakly interacting mode can be used for precise external manipulations and measurements. In the context of quantum information science, strong interactions are required to implement fast quantum gates, and long-term storage is achieved in the noninteracting regime (*2*, *3*).

Cold atomic gases are a fruitful platform for such studies. They permit one to perform experiments under well-understood and controlled conditions. Tuning the strength of short-range interactions can be accomplished by using magnetic and optical Feschbach resonances (*1*, *4*). Resonant optical driving of an atomic gas between the ground level and a high-lying Rydberg level is a particularly promising setting for studies of many-body systems with strong, long-range interactions (*5*–*13*). The interaction strength between atoms can vary enormously depending on the principal quantum number n of the atomic level. An important manifestation of Rydberg-level interactions is excitation blockade, in which an atom promoted to a Rydberg level shifts the energy levels of nearby atoms, suppressing their excitation. Previously, excitation blockade has been used to prepare entangled states of two isolated atoms (*14*, *15*) and has also been observed in atomic gases (*16*–*23*). However, controlled creation and manipulation of collective quantum excitations would open the door to investigations of interacting bosonic and fermionic fields, simulations of engineered quantum systems, and generation of complex entangled states of matter and light (*5*–*13*). Encoding of quantum information into symmetrized many-atom quantum states, or spin waves, is particularly attractive because discrimination against various types of noise is built into the manipulation and measurement protocols (*24*–*26*). Atomic spin waves can be efficiently mapped onto light fields, making such systems naturally suited for distribution of quantum information among remote locations.

A small size of the atomic ensemble is a prerequisite for complete suppression of multiply excited spin waves. The ensemble should also have a sufficiently large optical depth to couple the atomic spin wave to the retrieved light field. To create such a small and dense ensemble, we loaded laser-cooled ^{87}Rb atoms into a one-dimensional (1D) optical lattice formed by a retro-reflected (782-nm wavelength) light beam with Gaussian $1/e^2$ waists of $w_y = 15$ μm and $w_z = 55$ μm along the y and z dimensions, respectively (Fig. 1A). The geometry of the lattice and of the excitation beams was chosen so that the ensemble volume is determined by the $w_e = 9$ μm waists of the excitation beams in two dimensions (x and z) and the 15 μm lattice waist in the third (y). Atoms are prepared in the $|5s_{1/2}, F = 2, m_F = 0\rangle$ state by means of optical pumping in a magnetic bias field $B_0 = 4.3$ G applied along the z axis. After preparation, the lattice is turned off in order to avoid differential light shifts, and a 2.5-μs-long experimental cycle is repeated for a period of 200 μs, limited by thermal expansion of the temperature (T) ≅ 10 μK atomic cloud. A τ_e = 200-ns-long period of two-photon excitation by nearly counterpropagating 795 nm (Ω_1) and 475 nm (Ω_2) laser fields tuned near the two-photon $|5s_{1/2}, F = 2\rangle \leftrightarrow |ns_{1/2}\rangle$ resonance creates an optical-frequency spin wave between the ground and the Rydberg levels (Fig. 1B).

After a controlled storage period T_s, a 475-nm retrieval field (Ω_3) resonant with the $|ns\rangle \leftrightarrow |5p_{1/2}\rangle$ transition illuminates atoms for a 1-μs period. This read-out laser pulse converts the spin wave into the retrieved field, which is coupled into a single-mode fiber followed by a beam-splitter and a pair of single-photon detectors, D_1 and D_2. Statistics of the retrieved spin wave is inferred from the distribution of the photoelectric detection events (*27*).

The sum of the photoelectric detection event probabilities at the two detectors, $P = p_1 + p_2$, is shown in Fig. 2A as a function of the two-photon detuning Δ_2 from level $|90s_{1/2}\rangle$. The two peaks correspond to $m = \pm 1/2$ Zeeman sublevels split by the bias field B_0; the width of the peaks, $\gamma \approx 2\pi \times 5$ MHz, is determined by the spectral widths of the excitation laser pulses. In Fig. 2B, the time-resolved photoelectric detection probability P is shown for values of n between 50 and 102. With a $\sim n^{-3/2}$ scaling of the dipole matrix element—and, hence, of the Rabi frequency Ω_3 for

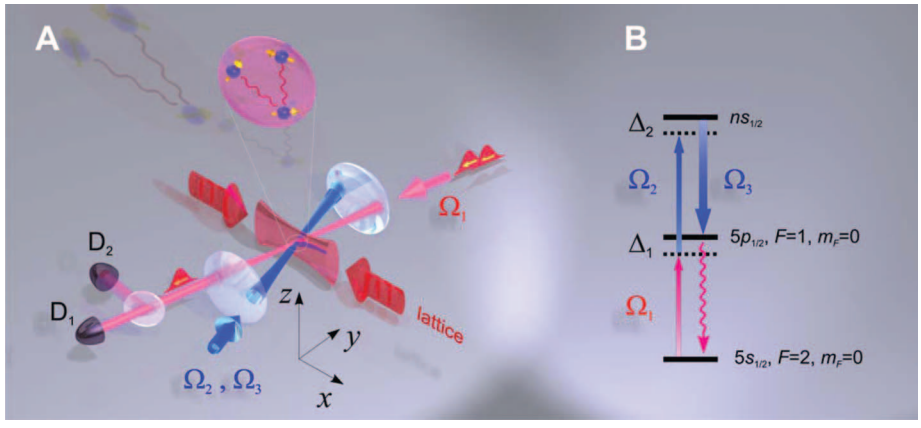

Fig. 1. (**A**) A cold dense sample of atomic ^{87}Rb is prepared in a 1D optical lattice. The lattice is turned off for the experimental sequence, in which nearly counterpropagating 795-nm (Ω_1) and 475-nm (Ω_2) light fields excite a spin wave between the ground $|5s_{1/2}\rangle$ and a Rydberg $|ns_{1/2}\rangle$ level. After a variable delay, a read-out pulse of 475-nm light (Ω_3) converts the Rydberg spin wave into a light field. A Hanbury Brown-Twiss setup of a beamsplitter (BS) followed by two detectors D_1 and D_2 is used to measure the second-order intensity correlation function $g^{(2)}(0)$ of the idler field. (**B**) Relevant ^{87}Rb energy levels. Electronic, hyperfine, and Zeeman quantum numbers are shown. The detuning from the intermediate $|5p_{1/2}\rangle$ level is $\Delta_1 = -40$ MHz; the detuning Δ_2 is varied for the data in Fig. 2A, otherwise it is fixed at the two-photon resonance $|5s_{1/2}, F = 2\rangle \leftrightarrow |ns_{1/2}, m = \pm 1/2\rangle$ between the ground level and one of the Zeeman sublevels of the Rydberg level ($|\Delta_2| \approx 6$ MHz).

School of Physics, Georgia Institute of Technology, Atlanta, GA 30332–0430, USA.

*To whom correspondence should be addressed. E-mail: alex.kuzmich@physics.gatech.edu

Downloaded from www.sciencemag.org on May 20, 2012

the $|5p_{1/2}\rangle \leftrightarrow |ns_{1/2}\rangle$ transition—the retrieved field duration increases with n for a fixed power (18 mW) of the 475-nm read-out field.

In Fig. 2C, P is shown as a function of the two-photon excitation pulse area $\theta \equiv \Omega\tau_e$ for n = 74, 81, and 90, where the peak two-photon Rabi frequency is $\Omega \cong (\Omega_1\Omega_2)/(2\Delta_1)$ in the limit $\Omega_{1,2} << \Delta_1$. In the case of strong excitation blockade, collective Rabi oscillations occur even for inhomogeneous atom-light coupling (*28*). Technical sources of dephasing, such as laser linewidth, ac Stark shifts, and atom number fluctuations, are expected to reduce P to half of its maximum value as θ is increased. In contrast, in Fig. 2C we observe a decay of P to 0, with no revivals. These observations are consistent with the dephasing of multiply excited spin waves (*13*). The data for n = 90 are fit with a function $\zeta\mathcal{P}\theta^2\exp(-\mathcal{P}\theta^2)$, where ζ = 0.060(1) and $\mathcal{P}$ = 51(1) are adjustable parameters. The choice of the fit function is suggested by a model with Poisson spin-wave excitation statistics (*13*, *29*). Within the model, ζ corresponds to the overall measured retrieval and detection efficiency for the spin-wave excitation, whereas the maximum photoelectric detection probability is $P_m = \zeta/e$.

It is instructive to compare the strongly interacting regime to the ideal limit of a noninteracting ensemble, in which each atom undergoes a Rabi oscillation between the ground level $|5s_{1/2}\rangle$ and the Rydberg level $|ns_{1/2}\rangle$ with the position-dependent two-photon Rabi frequency $\Omega(\mathbf{r})$. Atoms in a sufficiently low-n Rydberg level may be used to approximate this ideal situation. In Fig. 2D, $P/\mathcal{T}$ is displayed as a function of θ both for high- and low-n Rydberg levels. The retrieved field is attenuated (for low-n) by a factor $1/\mathcal{T}$ to prevent saturation of the single-photon detectors D_1 and D_2. The weakly interacting (low-n) regime is represented by measurements with levels $|19s_{1/2}\rangle$ and $|21s_{1/2}\rangle$ ($\mathcal{T}_{19,21}$ = 0.05). The maximum photoelectric detection probability P_m and the corresponding pulse area θ_m are lower for n = 21 than for n = 19, which is indicative of interaction-induced excitation suppression. Results for n = 74, 81, and 90 ($\mathcal{T}_{74,81,90}$ = 1) suggest that for such high n, both P_m and θ_m approach asymptotic values. This would be expected if only a single retrievable excitation is generated in the entire ensemble. In this picture, the effective number of atoms $\mathcal{N}$ in the ensemble is proportional to the ratio of $P_m/\mathcal{T}$ for n = 19 and n = 90, giving $\mathcal{N} \cong 5 \times 10^2$. Collectively, enhanced coupling of the driving laser fields to the singly excited spin wave implies $\mathcal{N} \sim [\theta_m(n = 19)/\theta_m(n = 90)]^2 \cong 6 \times 10^2$. In the absence of data for $n < 19$, these values should be considered as low-end estimates of $\mathcal{N}$.

The single-photon character of the retrieved field was explicitly confirmed by cross-correlating the photoelectric counting events at detectors D_1 and D_2 as a function of time delay, as shown for upper-level $|102s_{1/2}\rangle$ in Fig. 3, inset. The observed coincidences around zero time delay are strongly suppressed, providing evidence for the quantum nature of the emitted light. We further investigated the transition to the regime of strongly interacting spin waves by measuring the second-order intensity correlation function at zero delay $g^{(2)}(0)$ (*27*) as a function of effective principal quantum number $n^* = n - \delta_s$ (Fig. 3). Here, δ_s = 3.13 is the s-wave quantum defect for Rb. As n^* is increased, interaction-induced suppression of spin waves with more than one Rydberg atom sets in, with the transition to the single retrievable excitation regime occurring for $n \sim 60$ to 70. The transition is associated with the interaction strength scaling as n^4/R^3 in the dipole-dipole regime for $R \lesssim R_c$ and as n^{11}/R^6 in the van der Waals regime for $R \gtrsim R_c$. Here, R_c is the critical inter-atom distance (*2*). For $n \lesssim 60$, van der Waals interactions are

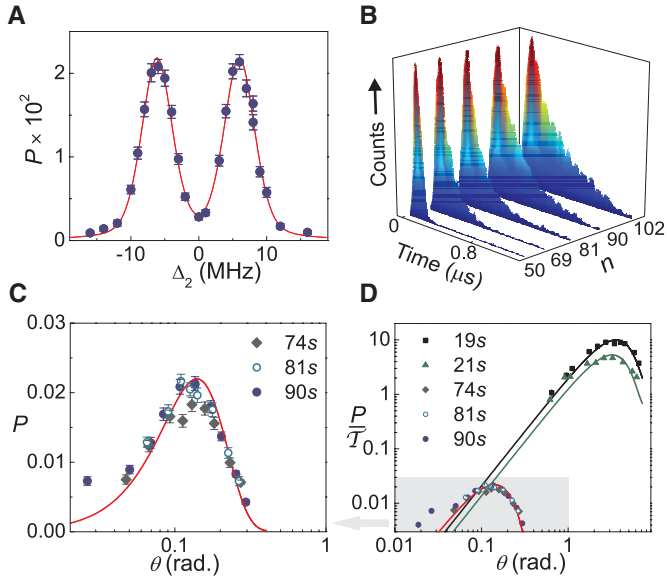

Fig. 2. (**A**) Probability P of photoelectric detection event per trial as a function of two-photon detuning Δ_2 shows the $m = \pm 1/2$ Zeeman components of level $|90s_{1/2}\rangle$ split by the bias field B_0. The solid curve is a pseudo-Voigt fit. (**B**) Normalized temporal profiles of the retrieved field for upper levels $|ns_{1/2}\rangle$ for n between 50 and 102, with a fixed power of the retrieval field Ω_3. (**C**) P as a function of (single-atom) two-photon excitation pulse area θ for T_s = 0.4 μs: solid circles for $|90s_{1/2}\rangle$, open circles for $|81s_{1/2}\rangle$, and diamonds for $|74s_{1/2}\rangle$ upper level. The solid curve is a fit of the form $\zeta\mathcal{P}\theta^2\exp(-\mathcal{P}\theta^2)$ to the $|90s_{1/2}\rangle$ data. (**D**) $P/\mathcal{T}$ as a function of θ. Results plotted in (C) are shown together with additional data for levels $|19s_{1/2}\rangle$ and $|21s_{1/2}\rangle$. The data for n = 19 and n = 21 are taken with the retrieved field attenuated by a factor $1/\mathcal{T}_{19,20}$ = 20 to avoid detector saturation, whereas for n = 74, 81, and 90, no attenuation is used ($\mathcal{T}_{74,81,90}$ = 1). The n = 19 and n = 21 data are fitted with a function accounting for averaging of sinusoidal oscillations of the retrievable spin-wave amplitude across the Gaussian transverse spatial profiles of $\Omega_{1,2}(\mathbf{r})$ (*27*). Error bars represent ±1 SD ($\sqrt{M}$) for M photoelectric counting events.

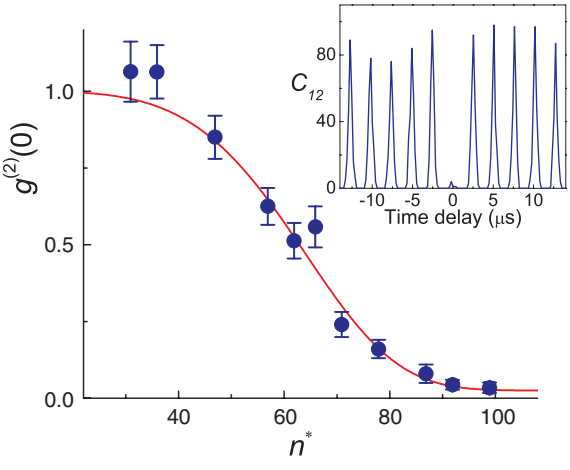

Fig. 3. Measured second-order intensity correlation function at zero time delay $g^{(2)}(0)$ as a function of the effective principal quantum number $n^* = n - \delta_s$ of the upper-level $|ns_{1/2}\rangle$ for $T_s \cong 0.3$ μs. For $n^* > 70$, the data are taken at θ_m, whereas for $n^* \lesssim 70$, the values of θ are chosen to keep P between 0.02 and 0.03 (Fig. 2D). The solid line is a fit of the form $g^{(2)}(0) = [1 - g^{(2)}_{bg}]\exp[-(n^*/n^*_0)^\alpha] + g^{(2)}_{bg}$, with best-fit values α = 4.7(4) and n^*_0 = 67(1). (**Inset**) Cross-correlated coincidence counts C_{12} as a function of time delay for upper-level $|102s_{1/2}\rangle$. Error bars represent ±1 SD ($\sqrt{M}$) for M photoelectric counting events.

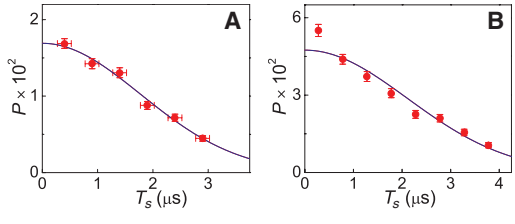

Fig. 4. Photoelectric detection probability P as a function of the storage time T_s. (**A**) For upper-level $|90s_{1/2}\rangle$. (**B**) For upper-level $|34s_{1/2}\rangle$. Experimental data showing decay are fitted with a Gaussian function $\exp(-T_s^2/\tau^2)$, with best-fit values τ_{90} = 2.5(1) μs and τ_{34} = 3.0(1) μs. The vertical error bars represent ±1 SD ($\sqrt{M}$) for M photoelectric counting events. The horizontal error bars represent the lengths of the retrieved light pulses.

Downloaded from www.sciencemag.org on May 20, 2012

relevant because $R_c \lesssim 3$ μm is sufficiently smaller than the ~10-μm sample size. In contrast, for $n \sim 100$ dipole-dipole interactions become operational as $R_c \cong 10$ μm.

High-quality single-photon statistics are observed for $n \gtrsim 90$. For an ideal single-photon source, $g^2(0)$ would be nonzero only because of background counts on $D_{1,2}$. The measured background photoelectric count probability is $P_B = 2.5 \times 10^{-4}$ for the 0.74-μs detection window, with $P_D = 0.55P_B$ resulting from detector dark counts, and the remainder caused by various scattered light sources. The measured value of $g^{(2)}(0) = 0.040(14)$ for level $|102s_{1/2}\rangle$ is consistent with a lower bound of $g^{(2)}_{bg} = 0.025(1)$ because of background counts. A dearth of excess coincidences indicates a strong suppression of spin waves with more than one excitation. Both excitation blockade and spin-wave dephasing can contribute to suppression of two-photon events. As a step to separating the roles of the two mechanisms, we used $|nd_{3/2}\rangle$ upper levels for which the excitation blockade is expected to break down because of a pronounced angular dependence of interactions between atom pairs (*2*). The observed strong suppression of two-photon events [$g^{(2)}(0) = 0.066(38)$ for level $|88d_{3/2}\rangle$ and $g^{(2)}(0) = 0.075(26)$ for level $|100d_{3/2}\rangle$] suggests a substantial role of spin-wave dephasing in our experiment.

The measured probability of photoelectric detection per trial P was 2 to 3% for the data in Fig. 3. When normalized by the 0.52 measured optical transmission from the sample to the detectors and 0.55 single-photon detector efficiency, $P_m(n = 90) = 2.8\%$ corresponds to $\epsilon \approx 0.10$ single-photon generation efficiency. This is limited by several experimental imperfections. The retrieval field Ω_3 has the same spatial mode as the excitation field Ω_2. Higher available laser power and a larger spatial mode for Ω_3 are expected to increase ϵ. A smaller sample should lead to a pronounced excitation blockade, whereas a medium-to-low finesse cavity may increase spin wave retrieval efficiency. As it is, the single-photon source has lower $g^{(2)}(0)$ and higher P and is more than three orders of magnitude faster than a deterministic single-photon source (*30*) based on the Duan, Lukin, Cirac, and Zoller protocol (*24*).

To evaluate coherence properties of the created optical spin-wave excitations, the retrieved signal is measured as a function of storage time T_s. For this data, an extended 5-μs-long timing sequence was used. For $n = 90$, the signal is shown in Fig. 4A. The observed $1/e$ coherence time $\tau_{90} = 2.5(1)$ μs is consistent with the decoherence expected from atomic motion, which smears the phase grating imprinted on the atoms during the excitation. The period of the spin wave formed by counterpropagating Ω_1 and Ω_2 fields is $\Lambda \cong 1$ μm. The expected motional coherence time is $\tau \cong \Lambda/(2\pi v) \cong 5$ μs, where $v = (k_B T/M)^{1/2} \cong 3$ cm/s is the atomic velocity, k_B is Boltzmann's constant, $T = 10$ μK is the atomic temperature, and M is the mass of ^{87}Rb. In principle, there may be additional sources of decoherence for highly excited Rydberg levels, such as stray electric fields. To test this, a similar measurement was performed for $n = 34$ (Fig. 4B). The excitation level was kept low to preclude influence of interactions of multiply excited spin waves. The somewhat higher value of the observed coherence time $\tau_{34} = 3.0(1)$ μs may indicate a possible contribution to τ_{90} of Rydberg atom interactions with other atoms or external electric fields. However, atomic motion appears to provide the dominant contribution to the observed decoherence, which is also confirmed by lower values of τ in measurements with higher sample temperatures. In the future, it should be possible to reduce motional dephasing by further cooling. One may also use multi-photon excitation to produce larger-period spin waves, which are less susceptible to atomic motion (*13*), or pin the spin wave in a magic-wavelength (for the ground-Rydberg transition) optical lattice (*31*).

We have shown that strong Rydberg-level interactions can be used for the fast preparation of single-quantum excitations of a cold atomic gas. Using two different spin waves within the same ensemble, each driven by an independent single-photon field Ω_1, a photon-photon quantum gate can be realized. This work can be extended to the creation of several entangled spin waves (*13*). This would also allow investigation of interacting fermionic and bosonic collective excitations (*8*). Entangled spin waves may also be mapped either onto long-lived atomic coherences or light fields, opening possibilities for scalable remote entanglement distribution (*10*, *13*).

References and Notes

1. I. Bloch, J. Dalibard, W. Zwerger, *Rev. Mod. Phys.* **80**, 885 (2008).
2. M. Saffman, T. G. Walker, K. Mølmer, *Rev. Mod. Phys.* **82**, 2313 (2010).
3. A. G. Radnaev *et al.*, *Nat. Phys.* **6**, 894 (2010).
4. M. W. Zwierlein, J. R. Abo-Shaeer, A. Schirotzek, C. H. Schunck, W. Ketterle, *Nature* **435**, 1047 (2005).
5. M. D. Lukin, M. Fleischhauer, R. Cote, *Phys. Rev. Lett.* **87**, 037901 (2001).
6. M. Saffman, T. G. Walker, *Phys. Rev. A* **72**, 042302 (2005).
7. M. Müller, I. Lesanovsky, H. Weimer, H. P. Büchler, P. Zoller, *Phys. Rev. Lett.* **102**, 170502 (2009).
8. B. Olmos, R. González-Férez, I. Lesanovsky, *Phys. Rev. Lett.* **103**, 185302 (2009).
9. H. Weimer, M. Müller, I. Lesanovsky, P. Zoller, H. P. Büchler, *Nat. Phys.* **6**, 382 (2010).
10. B. Zhao, M. Müller, K. Hammerer, P. Zoller, *Phys. Rev. A* **81**, 052329 (2010).
11. G. Pupillo, A. Micheli, M. Boninsegni, I. Lesanovsky, P. Zoller, *Phys. Rev. Lett.* **104**, 223002 (2010).
12. A. V. Gorshkov, J. Otterbach, M. Fleischhauer, T. Pohl, M. D. Lukin, *Phys. Rev. Lett.* **107**, 133602 (2011).
13. F. Bariani, Y. O. Dudin, T. A. B. Kennedy, A. Kuzmich, *Phys. Rev. Lett.* **108**, 030501 (2012).
14. E. Urban *et al.*, *Nat. Phys.* **5**, 110 (2009).
15. A. Gaëtan *et al.*, *Nat. Phys.* **5**, 115 (2009).
16. K. Singer, M. Reetz-Lamour, T. Amthor, L. G. Marcassa, M. Weidemüller, *Phys. Rev. Lett.* **93**, 163001 (2004).
17. D. Tong *et al.*, *Phys. Rev. Lett.* **93**, 063001 (2004).
18. T. C. Liebisch, A. Reinhard, P. R. Berman, G. Raithel, *Phys. Rev. Lett.* **95**, 253002 (2005).
19. T. Vogt *et al.*, *Phys. Rev. Lett.* **97**, 083003 (2006).
20. R. Heidemann *et al.*, *Phys. Rev. Lett.* **99**, 163601 (2007).
21. E. Brekke, J. O. Day, T. G. Walker, *Phys. Rev. A* **78**, 063830 (2008).
22. H. Kübler, J. P. Shaffer, T. Baluktsian, R. Löw, T. Pfau, *Nat. Photonics* **4**, 112 (2010).
23. J. D. Pritchard *et al.*, *Phys. Rev. Lett.* **105**, 193603 (2010).
24. L.-M. Duan, M. D. Lukin, J. I. Cirac, P. Zoller, *Nature* **414**, 413 (2001).
25. D. N. Matsukevich, A. Kuzmich, *Science* **306**, 663 (2004).
26. E. Brion, K. Mølmer, M. Saffman, *Phys. Rev. Lett.* **99**, 260501 (2007).
27. Supplementary materials are available on *Science* Online.
28. F. W. Cummings, A. Dorri, *Phys. Rev. A* **28**, 2282 (1983).
29. F. Bariani, T. A. B. Kennedy, *Phys. Rev. A* **85**, 033811 (2012).
30. R. Zhao *et al.*, *Nat. Phys.* **5**, 100 (2009).
31. S. Zhang, F. Robicheaux, M. Saffman, *Phys. Rev. A* **84**, 043408 (2011).

Acknowledgments: We thank F. Bariani, B. Kennedy, A. Radnaev, A. Zangwill, and C. Campbell for discussions. This work was supported by the Air Force Office of Scientific Research Atomic Physics Program, Quantum Memories Multidisciplinary University Research Initiative, and NSF.

Supplementary Materials

www.sciencemag.org/cgi/content/full/science.1217901/DC1
Supplementary Text
Fig. S1

14 December 2011; accepted 9 April 2012
Published online 19 April 2012;
10.1126/science.1217901

Water-Mediated Proton Hopping on an Iron Oxide Surface

Lindsay R. Merte,[1]* Guowen Peng,[2] Ralf Bechstein,[1] Felix Rieboldt,[1] Carrie A. Farberow,[2] Lars C. Grabow,[2]† Wilhelmine Kudernatsch,[1] Stefan Wendt,[1] Erik Lægsgaard,[1] Manos Mavrikakis,[2]‡ Flemming Besenbacher[1]‡

The diffusion of hydrogen atoms across solid oxide surfaces is often assumed to be accelerated by the presence of water molecules. Here we present a high-resolution, high-speed scanning tunneling microscopy (STM) study of the diffusion of H atoms on an FeO thin film. STM movies directly reveal a water-mediated hydrogen diffusion mechanism on the oxide surface at temperatures between 100 and 300 kelvin. Density functional theory calculations and isotope-exchange experiments confirm the STM observations, and a proton-transfer mechanism that proceeds via an H_3O^+-like transition state is revealed. This mechanism differs from that observed previously for rutile TiO_2(110), where water dissociation is a key step in proton diffusion.

The diffusion of hydrogen on oxide surfaces is an important process in a number of applications, including catalytic hydrogen evolution and reforming (*1*–*3*), photocatalytic dehydrogenation (*4*), the synthesis of metallic materials from oxide precursors (*5*),

Downloaded from www.sciencemag.org on May 20, 2012